Chemical Science

ROYAL SOCIETY OF CHEMISTRY

EDGE ARTICLE

View Article Online
View Journal

Cite this: DOI: 10.1039/d6sc01836j

All publication charges for this article have been paid for by the Royal Society of Chemistry

Received 4th March 2026
Accepted 25th March 2026

DOI: 10.1039/d6sc01836j

rsc.li/chemical-science

Stepwise B≡N bond cleavage by isocyanides: access to the 3-azaborole structural motif

Libo Xiang,†[a] Ka Ho Kwan,†[b] Yi Jing,[c] Junyi Wang,[d] Alexander Matler,[a] Xuenian Chen,[c] Zhenyang Lin *[b] and Qing Ye *[a]

The reaction of ^{TMS}oCb–B≡N–SiMe$_3$ (^{TMS}oCb = 1-trimethylsilyl-*ortho*-carboranyl) with the sterically demanding (2,4,6-tri-*tert*-butylphenyl)isocyanide enables the isolation of the corresponding 1 : 1 iminoborane-isocyanide adduct, a species considered to be the key intermediate in isocyanide-catalyzed dimerization. In sharp contrast, the less hindered isocyanides, namely (2,4,6-trimethylphenyl)isocyanide and (2,6-di-*iso*-propylphenyl)isocyanide, react with the *o*-carboranyl iminoborane in a 3 : 1 fashion. Two equivalents of isocyanide undergo a [2 + 1 + 1] cycloaddition with the B≡N triple bond to furnish a 1,2-azaborete-3,4-diimine four-membered ring, while the third equivalent coordinates to the boron center of the ring. Subsequent reduction with Mg or Ca induces selective insertion of this third isocyanide into the BN bond, generating an unprecedented 3-azaborolediide species. Single crystal structure characterization and quantum chemical calculations reveal that the negative charge is extensively delocalized onto the *o*-carborane cage. Theoretical studies further establish a clear mechanistic pathway for the entire transformation.

Introduction

Iminoboranes (R–B≡N–R′) feature a B≡N triple bond that is isoelectronic with a C≡C triple bond, and can therefore be regarded as "inorganic alkynes".[1] Due to the pronounced polarity of the B≡N bond, iminoboranes exhibit much higher reactivity than alkynes.[2] For example, they tend to undergo (cyclo)oligomerization. In addition, the boron center is electrophilic and readily forms adducts with various Lewis bases.[3] In addition, the B≡N triple bond of iminoboranes can react with the C≡C triple bond of alkynes under the assistance of rhodium, proceeding *via* a 1,2-azaborete intermediate to ultimately afford 1,4-azaborines or 1,2-azaborines products, which are BN-isosteres of benzene derivatives.[4] In these transformations, iminoboranes act as BN synthons.

On the other hand, isocyanides, analogous to CO, constitute an important class of C1 synthons. They are stronger σ-donors than CO and can act as Lewis bases to stabilize low-valent boron compounds.[5] In fact, isocyanides are sufficiently nucleophilic to attack the boron atom of the B≡N unit, thereby triggering follow-up reactions. Paetzold and co-workers carried out seminal work, showing that iminoboranes can react with isocyanides to afford various cyclic adducts.[6] In the presence of catalytic amounts of *t*BuNC, F_5C_6–B≡N–*t*Bu readily dimerizes to form the diazadiboretidine product (**I** in Fig. 1). Increasing the loading of *t*BuNC to one equivalent affords a 1,3-diaza-2,4-diboracyclopentane-type product (**II**). Further reaction of **II** with a second equivalent of isocyanide has not been reported. However, a 1 : 2 reaction between an iminoborane and an isocyanide has been achieved for the B-amino iminoborane Me_3-Si(*t*Bu)N–B≡N–*t*Bu, which reacts with two equivalents of (2,6-dimethylphenyl)isocyanide to form the 1,2-azaborete-3,4-diimine product (**III**). In 2022, our laboratory successfully synthesized the first *o*-carboranyl iminoborane, ^{TMS}*o*Cb–B≡N–R (^{TMS}*o*Cb = 1-trimethylsilyl-*ortho*-carboranyl, R = $SiMe_3$, *t*Bu), and demonstrated that it also undergoes isocyanide-catalyzed dimerization.[7] DFT calculations indicate that the 1 : 1 adduct formed between an iminoborane and an isocyanide is the key intermediate in this catalytic dimerization process.

In this context, curiosity has turned toward: (1) whether the reaction could be halted at the 1 : 1 adduct stage so that this key intermediate could be isolated; (2) whether the 1 : 1 adduct is also a key intermediate for the formation of **III**; and (3) whether **III** could undergo a further ring-expansion reaction with a third equivalent of isocyanide to afford new BN heterocycles, such as the azaboroles shown in Scheme 1.

Boroles (**IV** in Scheme 1) are boracycle derivatives of cyclopentadiene in which the saturated carbon position is replaced by a sp^2-hybridized boron with an empty p-orbital. are

[a]*Institute for Inorganic Chemistry and Institute for Sustainable Chemistry & Catalysis with Boron, Julius-Maximilians-Universität Würzburg, 97074 Würzburg, Germany. E-mail: qing.ye@uni-wuerzburg.de*

[b]*Department of Chemistry, The Hong Kong University of Science and Technology, Kowloon, Hong Kong. E-mail: chzlin@ust.hk*

[c]*College of Chemistry, Zhengzhou University, 450001, Zhengzhou, Henan, P. R. China*

[d]*Department of Chemistry, Southern University of Science and Technology, 518055, Shenzhen, Guangdong, P. R. China*

† These authors contributed equally to this work.

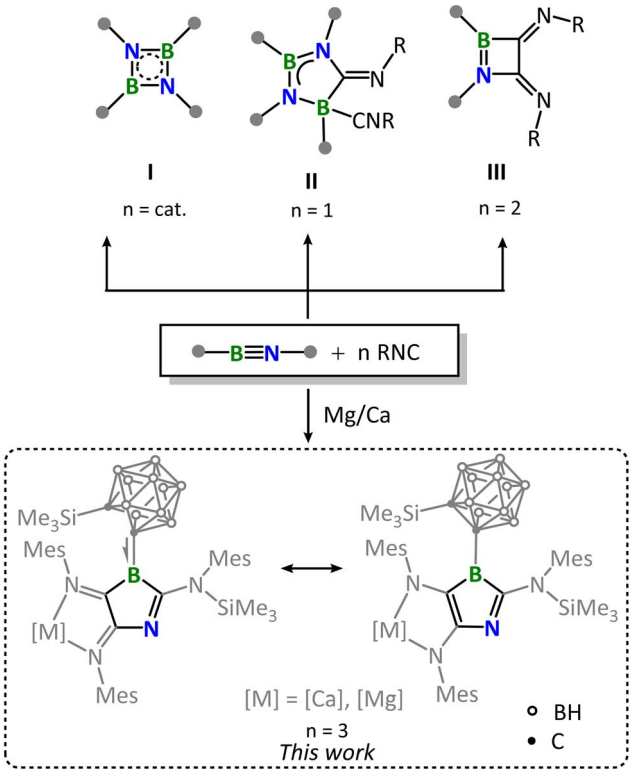

Fig. 1 Reactions between iminoboranes and isocyanides leading to 1,3,2,4-diazadiboretidines (I), 1,3-diaza-2,4-diboracyclopentanes (II), 1,2-azaborete-3,4-diimines (III) and 3-azaborolediides (this work). Mes = 2,4,6-trimethylphenyl.

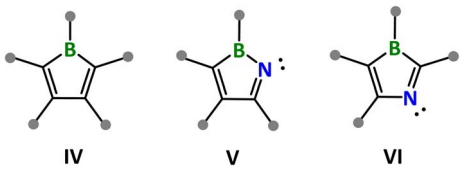

Scheme 1 Boroles (IV), 2-azaboroles (V), and 3-azaboroles (VI).

renowned for their 4π antiaromaticity, the electron deficiency of the boron center, and the resulting unique electronic properties and rich chemical reactivity (*e.g.* Lewis acid–base reaction, ring expansion, small-molecule activation, π-ligands in the formation of sandwich complexes).[8] Very recently, our laboratory successfully synthesized the first 2-azaborole (**V** in Scheme 1) derivatives featuring a $\sigma^2\pi^4$ electronic configuration *via* ring-expansion reactions of benzoborirene $C_6H_4\{BN(SiMe_3)_2\}$ with nitriles.[9] In contrast, 3-azaboroles (**VI** in Scheme 1) have not yet been reported. Herein, we report our progress toward the construction of the 3-azaborole structural motif using an *o*-carboranyl-substituted iminoborane as a BN synthon and isocyanides as C_1 synthons.

Results and discussion

To halt the reaction at the 1 : 1 adduct stage, a highly sterically demanding isocyanide is expected to play a crucial role. Such

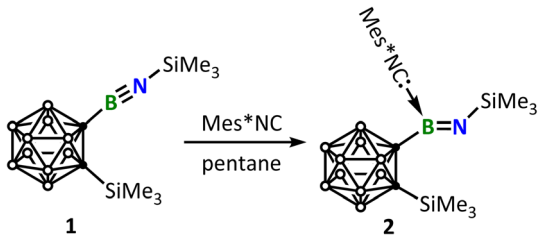

Scheme 2 Synthesis of isocyanide-iminoborane adduct **2**.

steric congestion would kinetically block both (i) cycloaddition between the 1 : 1 adduct and another free iminoborane molecule and (ii) further reaction of the adduct with a second equivalent of isocyanide to form **III**. Therefore, Mes*NC (Mes* = 2,4,6-tri-*tert*-butylphenyl) was chosen (Scheme 2). The reaction of iminoborane **1** with an equimolar amount of Mes*NC was monitored by the ^{11}B-NMR spectrum, which revealed a slight upfield shift from δ_B 13.5 (**1**)[7] to δ_B 13.4, accompanied by a color change from colorless to pale yellow. Orange single crystals suitable for X-ray diffraction analysis were obtained upon storing the light yellow pentane solution of the reaction mixture at −30 °C for 12 h. The solid-state structure unambiguously revealed a 1 : 1 adduct between **1** and Mes*NC (Fig. 2). The B1–N1 bond of (1.302(13) Å) is elongated by *ca.* 10 pm compared to that in **1** (1.220(2) Å), indicating a transformation from a B≡N triple bond to a B=N double bond. In line with this observation, while the IR spectrum of **1** shows a characteristic B≡N stretching vibration at 1976 cm^{-1},[7] the BN stretching vibration of **2** appears at 1605 cm^{-1}, as supported by the corresponding ^{10}B isotopic shift (Fig. S25).[7] The C2–B1 bond distance of 1.639(13) Å is comparable to the $C_{carbene}$–B bond distance of 1.626(3) Å observed in ^{Me}I*i*Pr-**1** adduct (^{Me}I*i*Pr = 1,3-di-*iso*-propyl-4,5-dimethyl-imidazole-2-ylidene).[10]

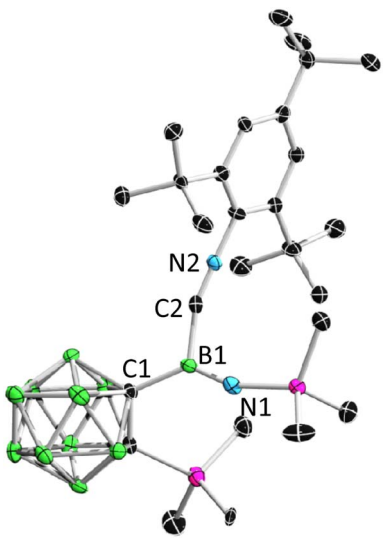

Fig. 2 Single crystal structure of **2**. Hydrogen atoms have been removed for clarity. Thermal ellipsoids are drawn at the 50% probability level. Selected bond lengths (Å) and angles (deg): B1–N1 1.305(3), B1–C2 1.635(3), C2–N2 1.152(3), C1–B1–N1 130.0(2), B1–C2–N2 163.4(2).

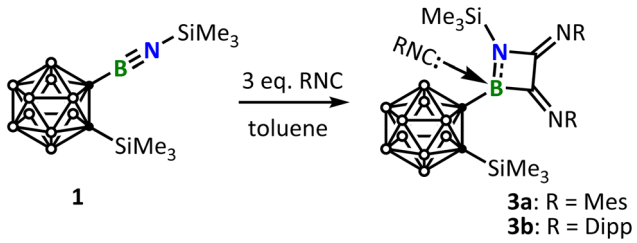

Scheme 3 Synthesis of **3**.

Next, we examined MesNC (Mes = 2,4,6-trimethylphenyl), which features reduced steric hindrance. In stark contrast, the treatment of **1** with one equivalent of MesNC resulted in a mixture consisting of considerable amount of unreacted **1** and a new species **3a**, which according to the ^{1}H-NMR spectrum, should be composed of one equivalent of **1** and three equivalents of MesNC. Addition of a second equivalent of MesNC led to an increased portion of **3a**. Complete consumption of **1** was only achieved upon the addition of a third equivalent of MesNC, whereupon **1** was quantitatively converted into **3a**. This further corroborates that **1** reacted with MesNC in a 1 : 3 ratio (Scheme 3). Yellow single crystals of **3** suitable for X-ray diffraction analysis were obtained upon slow diffusion of pentane into the concentrated toluene solution of **3** at −30 °C. Likewise, the reaction employing DippNC (Dipp = 2,6-di-*iso*-propylphenyl), an isocyanide whose steric demand lies between that of Mes*NC and MesNC, furnished the same kind of product **3b**, though in a lower yield.

The single crystal structure is depicted in Fig. 3, suggesting that **3** should arise from the initial reaction of **1** with two equivalents of RNC (R = Mes, **3a**; R = Dipp, **3b**) to afford the 1,2-azaborete-3,4-diimine (**III**), followed by adduct formation with a third equivalent of RNC. The BNCC four-member ring is slighted twisted as indicated by the dihedral angles B1–C2–C3–N1 of **3a** (−12.916°) and **3b** (−12.162°), respectively. The exocyclic C2–N2 (**3a**, 1.2656(18) Å and **3b**, 1.272(2) Å) and C3–N3 (**3a**, 1.2713(18) Å and **3b**, 1.2680(19) Å) bond lengths fall in the range of C=N double bonds. The major structural difference between **3a** and **3b** is that **3a** exhibits pronounced Mes–Mes π–π stacking interactions with a centroid-to-centroid distance of 3.514 Å, whereas in **3b**, the two Dipp groups adopt an orientation away from each other due to significant steric repulsion between their *iso*-propyl substituents (Fig. 3).

The calculated mechanistic pathway for the formation of compound **3′**, a model compound for **3**, is presented in Fig. 4. The process begins with the coordination of an isocyanide molecule to the compound **1** at the iminoborane boron center, forming the adduct **Int1**. Starting from **Int1**, an alternative route involving C–C coupling with a second PhNC molecule *via* nucleophilic attack on the coordinated carbon was examined, but found to be energetically unfavourable (see the blue energy profile in Fig. 4). Instead, **Int1** undergoes structural rearrangement to form **Int2**, a three-membered ring species generated through $N_{(iminoborane)}$–$C_{(coordinated\ isocyanide)}$ bond formation. Subsequent coordination of another PhNC molecule to the iminoborane boron center in **Int2**, accompanied by BN π-bond cleavage, yields **Int3**. From **Int3**, a 1,2-carbon shift produces the four-membered ring **Int4**, and coordination of a third PhNC molecule ultimately affords compound **3′**. The overall barrier for this transformation is 20.5 kcal mol^{-1} in Gibbs free energy, with a reaction free energy of −12.8 kcal mol^{-1}. The rate-determining transition state corresponds to the coordination of the second PhNC molecule.

α-Diimines are known to undergo two-electron reduction to form α-diamides.[11] In our earlier work, this approach enabled the synthesis of an antiaromatic benzo-fused borolediide.[12] Thus, the diimine function in **3** immediately caught our attention. To this end, a THF solution of **3a** was stirred with one equivalent of Mg(An)THF$_3$ (An = anthracene) or with calcium metal at room temperature, resulting in a color change from yellow to deep purple. The reaction with Mg(An)THF$_3$ proceeds much faster due to its homogeneous reaction nature, being completed within hours, whereas the reaction with calcium requires several days (Scheme 4). The ^{11}B-NMR spectra displayed the formation of new boron-containing species **4a** (δ_B

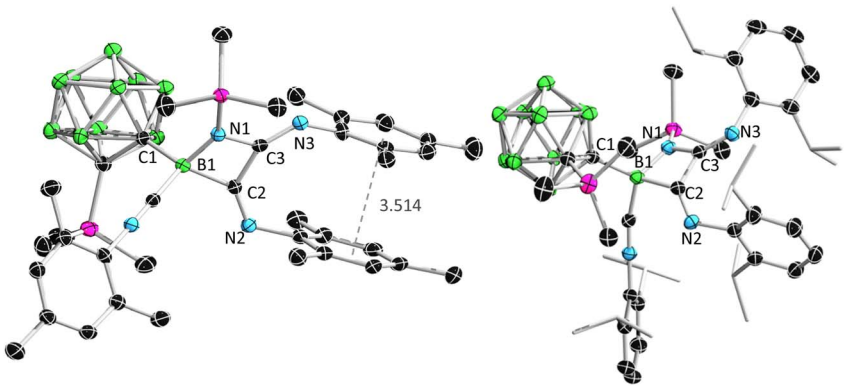

Fig. 3 Solid-state structure of **3a** (left), **3b** (right). Hydrogen atoms have been removed for clarity. Thermal ellipsoids are drawn at the 50% probability level. Selected bond lengths (Å) and angles (deg): for **3a**, B1–C1 1.657(2), B1–N1 1.5446(18), B1–C2 1.644(2), C2–C3 1.5333(18), N3–C3 1.2713(18), C2–N2 1.2656(18), C3–N3 1.2713(18), C2–B1–N1 83.77(10); for **3b**, B1–C1 1.652(2), B1–N1 1.567(2), B1–C2 1.645(2), C2–C3 1.498(2), N3–C3 1.2680(19), C2–N2 1.272(2), C3–N3 1.4230(19), C2–B1–N1 83.34(11).

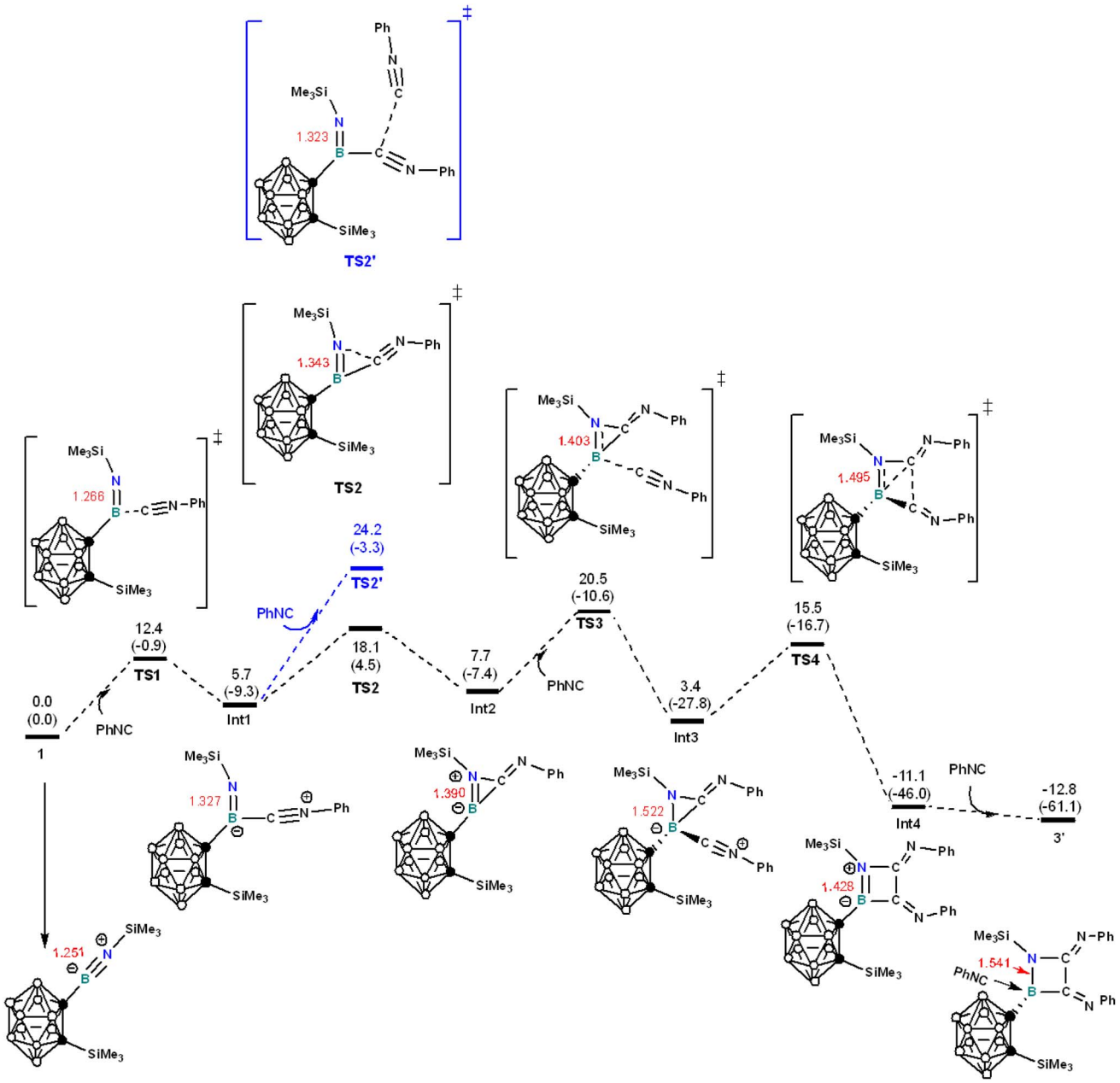

Fig. 4 Energy profile calculated for the formation of compound 3′, a model compound for 3. Selected B–N bond distances (Å) marked in red are provided, illustrating the change in the bonding character along the reaction pathway. Relative Gibbs free energies and electronic energies (in parentheses) are given in kcal mol^{-1}.

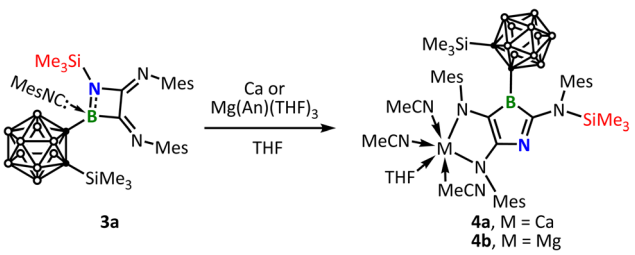

Scheme 4 Synthesis of 4.

29.8) and **4b** (δ_B 26.9), respectively. After removal of the solvent and thorough washing with hexane, the residue was extracted with acetonitrile and crystallized at −30 °C, yielding deep purple single crystals suitable for X-ray diffraction analysis (Fig. 5). The solid-state structure reveals the presence of coordinated acetonitrile ligand, which originates from the recrystallization solvent. The atom connectivity reveals that **3a** has indeed undergone a two-electron reduction. More interestingly, the reduction triggers a selective insertion of the coordinated isocyanide into the BN bond, accompanied by migration of the silyl group (marked in red in Scheme 4) from the ring nitrogen

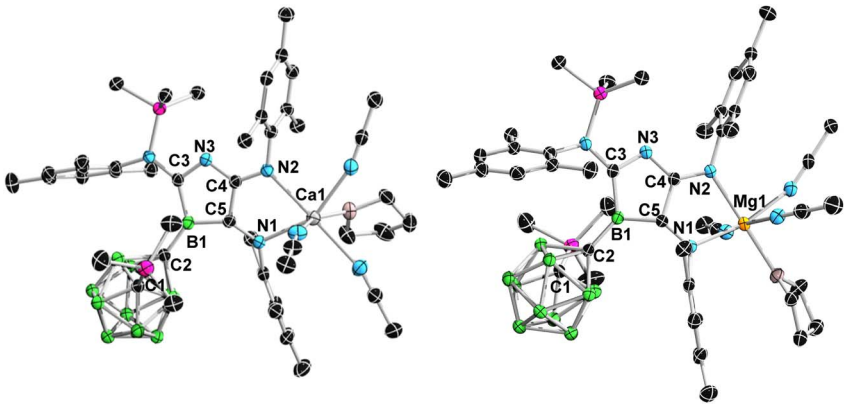

Fig. 5 Solid-state structure of **4a** (left), **4b** (right). Hydrogen atoms have been removed for clarity. Thermal ellipsoids are drawn at the 50% probability level. Selected bond lengths (Å) and angles (deg): for **4a**, B1–C2 1.485(4), C2–C1 2.436, C5–C4 1.515(3), C5–N1 1.314(3), C4–N2 1.315(3), C3–N3 1.363(3), B1–C5 1.562(4), B1–C3 1.594(3), N3–C4 1.347(3), C5–B1–C3 98.63(13), Ca1–N1 2.449(2), Ca1–N2 2.4002(18); for **4b**, B1–C2 1.485(2), C2–C1 2.474, C5–C4 1.513(2), C5–N1 1.319(2), C4–N2 1.301(2), C3–N3 1.356(2), B1–C5 1.561(4), B1–C3 1.601(2), N3–C4 1.357(2), C5–B1–C3 98.72(19), Mg1–N1 2.1439(14), Mg1–N2 2.1404(14).

atom to the nitrogen of the inserted isocyanide. Accordingly, at first glance, the crystal structure overall features an unprecedented 3-azaborole core (**VI** in Scheme 1). Further analysis of bond lengths and angles, such as the significantly elongated cage C–C distances (**4a**, 2.436 Å; **4b**, 2.474 Å), indicates pronounced negative hyperconjugation between the *o*-carborane moiety and the 3-azaborolediide unit in **4a**/**4b**. This is primarily manifested in the perpendicular orientation of the 3-azaborolediide fragment with respect to the C–C bond of the *o*-carborane cage (Fig. 6), which facilitates optimal overlap between the π orbitals of the 3-azaborole ring and the σ* antibonding orbital of the carborane C–C bond.[13] In addition to the direct population of the antibonding orbital by chemical reduction,[14d-f] elongation of the cage C–C bonds arising from negative hyperconjugation has in fact also been observed in 1,2-diamino-*o*-carboranes,[14a,b] 1-imino-*o*-carboranes[14c] and *o*-carboranyl-substituted three-coordinate borane radical anion.[13a] In addition, the B1–$C_{carborane}$ bond is notably shortened (**3a**, 1.657(2) Å; **4a**, 1.485(4) Å; **4b**, 1.485(2) Å), further corroborating the presence of the negative hyperconjugation with the *o*-carborane moiety acting as an electron acceptor.

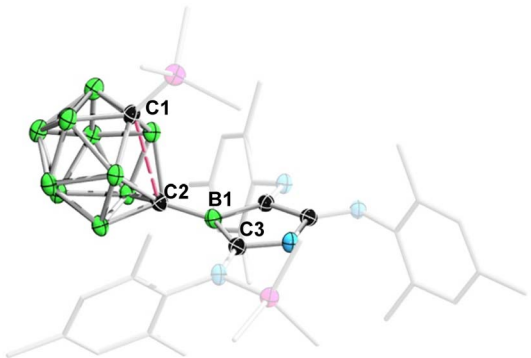

Fig. 6 Molecular structure of **4** highlighting the near-perpendicular orientation of the 3-azaborolediide fragment relative to the C–C bond of the *o*-carborane cage. Thermal ellipsoids are set at the 50% probability level. For clarity, hydrogen atoms, the [M] fragment and some of the ellipsoids are omitted. Selected angles (deg): for **4a**, C1–C2–B1–C3 100.070; for **4b**, C1–C2–B1–C3 99.320.

The calculated mechanistic pathway for the formation of compound **4a′** is presented in Fig. 7. The process begins with the reduction of **3′**, resulting in the formation of **Int5** which features N,N-coordination of the calcium ion. This formal two-electron reduction cleaves the two C=N π bonds in **3′** and generates a new C=C π bond, accompanied by metal coordination. The reaction is associated with a free energy change of 68 kcal mol^{-1}, indicating substantial gain in thermodynamic stability upon reduction. Starting from **Int5**, a 1,2-nitrogen shift expands the four-membered ring to yield **Int6**, a five-membered-ring intermediate with an envelope conformation. Subsequent planarization of the ring in **Int6** leads to **Int7** which features extended π-conjugation across the five-membered framework. This transformation provides significant stabilization, with a computed free energy gain of 36.6 kcal mol^{-1} (**Int6** → **Int7**). Finally, a 1,3-silyl migration from **Int7** yields **4a′**, which can be described by two resonance structures, **4a′_closo** and **4a′_nido**, accounting for the observed C–C bond elongation in the product **4a**. The participation of the resonance structure **4a′_nido** is supported by the HOMO plot (Fig. S30), which clearly shows the C(cage)–B(exo) π-bonding character. The overall barrier for the transformation from **Int5** to compound **4a′** is 12.2 kcal mol^{-1} in Gibbs free energy, with a reaction free energy of −30.1 kcal mol^{-1}.

We have also examined the alternative pathway involving insertion of the third equivalent of isocyanide into the B–C bond of **Int5** (Fig. 7). Our calculations show that this pathway has a higher activation barrier by 11.7 kcal mol^{-1} compared to insertion into the B–N bond. This insertion corresponds to a 1,2-carbon migration. The results indicate that the more covalent nature of the B–C bond relative to the B–N bond makes the 1,2-carbon migration significantly more energetically demanding and therefore kinetically less favorable.

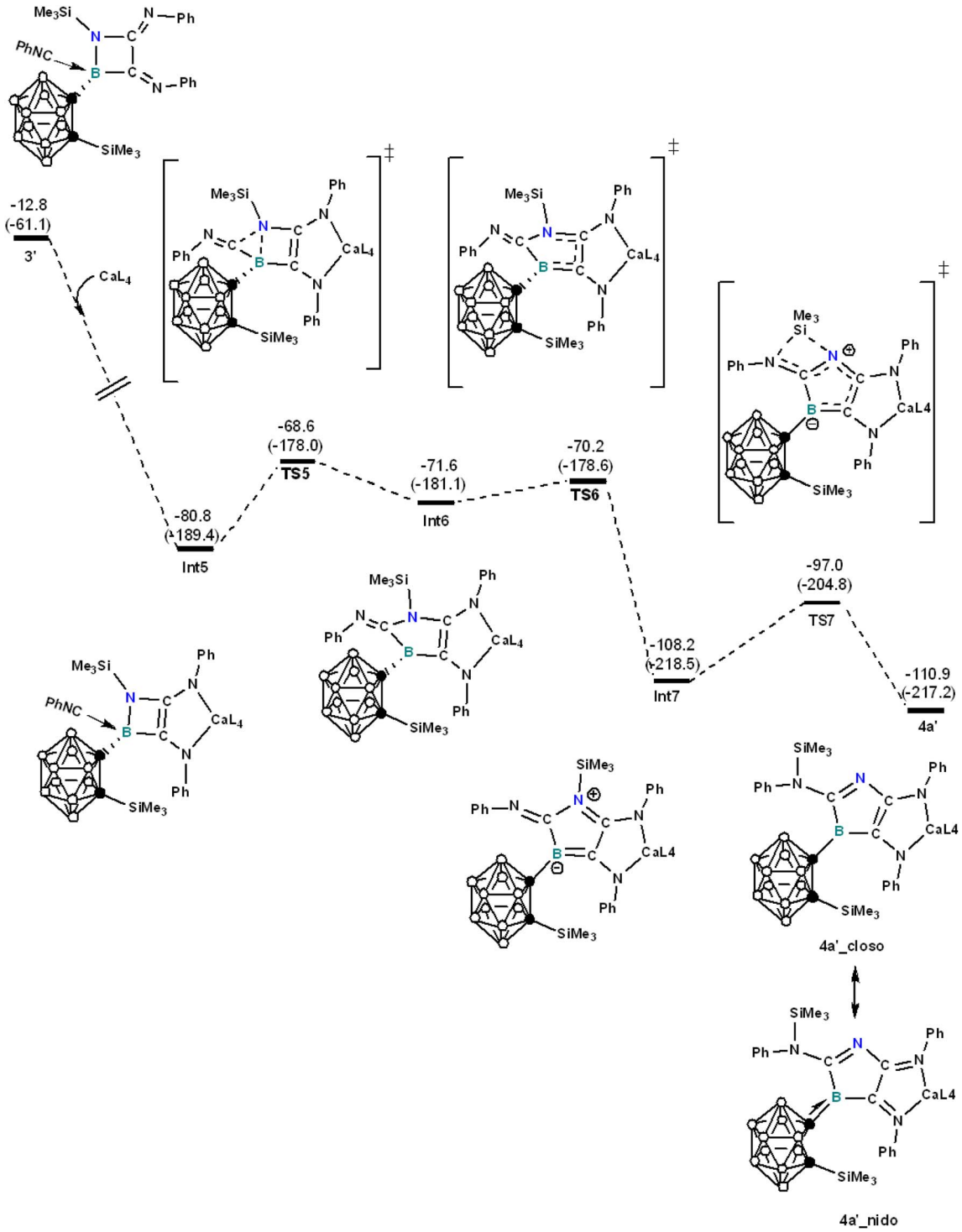

Fig. 7 Energy profile calculated for the formation of compound **4a′** *via* calcium metal reduction of **3′**. Relative Gibbs free energies and electronic energies (in parentheses) are given in kcal mol^{-1} "Ca + 2 THF + 2 MeCN" is abbreviated as CaL_4. L_4 represents 2 molecules of THF and 2 molecules of MeCN. Remark: The closo and nido-type drawings (**4a′_closo** and **4a′_nido**) serve as resonance representations of **4a′**. These do not correspond to isolable or independently optimizable species; rather, they illustrate complementary aspects of the delocalized bonding framework.

Additionally, we performed a Nucleus Independent Chemical Shift (NICS) analysis on **4a′** to evaluate the aromatic character of the edge-fused five-membered ring system. The NICS values at the geometric centers of the two rings, as well as at positions 1.0 Å above and below the ring planes, fall within a range centered at about −1.5 ppm, indicating that the fused-ring structure is non-aromatic.

Conclusion

In conclusion, we have identified a stepwise reaction pattern in which the B≡N triple bond of an *o*-carboranyl iminoborane engages sequentially with three equivalents of isocyanide to generate novel BN heterocycles. The first two equivalents undergo a [2 + 1 + 1] cycloaddition across the B≡N unit to afford a 1,2-azaborete-3,4-diimine four-membered ring. Under reducing conditions, the third equivalent inserts selectively into the BN bond, expanding the ring to a 3-azaborolediide species. Structural and computational analyses show that the strong inductive electron-withdrawing *o*-carboranyl substituent[15] participates in substantial electronic delocalization. Moreover, a sterically demanding isocyanide, *i.e.* Mes*NC, allowed the isolation of the corresponding 1 : 1 isocyanide-iminoborane adduct. This kind of 1 : 1 adduct species, previously suggested as the key intermediate in isocyanide-catalyzed iminoborane dimerization,[7] is further corroborated by quantum chemical calculations to be the intermediate leading to the formation of the 1,2-azaborete-3,4-diimine ring. The detailed computational study provides a clear mechanistic picture, illustrating how each elementary step transforms the B≡N triple bond and ultimately generates the 3-azaborolediide-type structure.

Conflicts of interest

There are no conflicts to declare.

Data availability

CCDC 2504504–2504508 contain the supplementary crystallographic data for this paper.[16a–e]

The data supporting this article have been included as part of the supplementary information (SI). Supplementary information: experimental details, synthesis, NMR and IR spectra, cyclic voltammetry, UV-vis spectra, computational details, crystallographic information, and additional characterization data. See DOI: https://doi.org/10.1039/d6sc01836j.

Acknowledgements

We thank Julius-Maximilians-Universität Würzburg (JMU) and the Research Grants Council of Hong Kong (HKUST 16301823) for financial support. We thank Christoph Mahler and Liselotte Michels for their help with testing high-resolution mass spectrometry (HRMS) and elemental analysis (EA), respectively.

Notes and references

1 L. Xiang, A. G. Albacar, J. Wang, A. Matler, T. Preitschopf, M. Finze and Q. Ye, *Organometallics*, 2025, **44**, 1756–1759.

2 (*a*) Y. Fan, J. Cui and L. Kong, *Eur. J. Org Chem.*, 2022, e202201086; (*b*) P. Paetzold, *Adv. Inorg. Chem.*, 1987, **31**, 123–170.

3 (*a*) H. Zhang, J. Wang, W. Yang, L. Xiang, W. Sun, W. Ming, Y. Li, Z. Lin and Q. Ye, *J. Am. Chem. Soc.*, 2020, **142**, 17243–17249; (*b*) L. Xie, J. Zhang, H. Hu and C. Cui, *Organometallics*, 2013, **32**, 6875–6878; (*c*) H. Braunschweig, W. C. Ewing, K. Geetharani and M. Schäfer, *Angew. Chem., Int. Ed.*, 2015, **54**, 1662–1665; (*d*) F. Dahcheh, D. W. Stephan and G. Bertrand, *Chem.–Eur. J.*, 2015, **21**, 199–204; (*e*) F. Dahcheh, D. Martin, D. W. Stephan and G. Bertrand, *Angew. Chem., Int. Ed.*, 2014, **53**, 13159–13163; (*f*) P. Cui, R. Guo, L. Kong and C. Cui, *Inorg. Chem.*, 2020, **59**, 5261–5265; (*g*) R. Guo, X. Zhang, T. Li, Q. Li, D. A. Ruiz, L. L. Liu, C. H. Tung and L. Kong, *Chem. Sci.*, 2022, **13**, 2303–2309; (*h*) A. Koner, T. Sergeieva, B. Morgenstern and D. M. Andrada, *Inorg. Chem.*, 2021, **60**, 14202–14211; (*i*) A. K. Swarnakar, C. Hering-Junghans, K. Nagata, M. J. Ferguson, R. McDonald, N. Tokitoh and E. Rivard, *Angew. Chem., Int. Ed.*, 2015, **54**, 10666–10669; (*j*) A. K. Swarnakar, C. Hering-Junghans, M. J. Ferguson, R. McDonald and E. Rivard, *Chem. Sci.*, 2017, **8**, 2337–2343.

4 (*a*) H. Braunschweig, A. Damme, J. O. C. Jimenez-Halla, B. Pfaffinger, K. Radacki and J. Wolf, *Angew. Chem., Int. Ed.*, 2012, **51**, 10034–10037; (*b*) H. Braunschweig, K. Geetharani, J. O. C. Jimenez-Halla and M. Schäfer, *Angew. Chem., Int. Ed.*, 2014, **53**, 3500–3504; (*c*) M. Schäfer, N. A. Beattie, K. Geetharani, J. Schäfer, W. C. Ewing, M. Krahfuß, C. Hörl, R. D. Dewhurst, S. A. Macgregor, C. Lambert and H. Braunschweig, *J. Am. Chem. Soc.*, 2016, **138**, 8212–8220; (*d*) M. Schäfer, J. Schäfer, R. D. Dewhurst, W. C. Ewing, M. Krahfuß, M. W. Kuntze-Fechner, M. Wehner, C. Lambert and H. Braunschweig, *Chem.–Eur. J.*, 2016, **22**, 8603–8609.

5 H. Braunschweig, R. D. Dewhurst, F. Hupp, M. Nutz, K. Radacki, C. W. Tate, A. Vargas and Q. Ye, *Nature*, 2015, **522**, 327.

6 C. Klöfkorn, M. Schmidt, T. Spaniol, T. Wagner, O. Costisor and P. Paetzold, *Chem. Ber.*, 1995, **128**, 1037–1043.

7 J. Wang, P. Jia, W. Sun, Y. Wei, Z. Lin and Q. Ye, *Inorg. Chem.*, 2022, **61**, 8879–8886.

8 (*a*) H. Braunschweig, I. Krummenacher and J. Wahler, *Adv. Organomet. Chem.*, 2013, **61**, 1–53; (*b*) J. He, F. Rauch, M. Finze and T. B. Marder, *Chem. Sci.*, 2021, **12**, 128–147; (*c*) A. Steffen, R. M. Ward, W. D. Jones and T. B. Marder, *Coord. Chem. Rev.*, 2010, **254**, 1950–1976; (*d*) X. Su, T. A. Bartholome, J. R. Tidwell, A. Pujol, S. Yruegas, J. J. Martinez and C. D. Martin, *Chem. Rev.*, 2021, **121**, 4147–4192.

9 (*a*) L. Tan, J. Chen, X. Liu, A. Matler, N. Schopper, M. Finze, Z. Lin and Q. Ye, *J. Am. Chem. Soc.*, 2024, **146**, 31681–31690; (*b*) S. Parua and Q. Ye, *Coord. Chem. Rev.*, 2026, **558**, 217742; (*c*) J. Wang and Q. Ye, *Chem.–Eur. J.*, 2023, **30**, e202303695.

10 L. Xiang, A. Matler, L. Tan and Q. Ye, *Dalton Trans.*, 2024, **53**, 11655–11658.

11 (*a*) M. Ma, L. Shen, H. Wang, Y. Zhao, B. Wu and X.-J. Yang, *Organometallics*, 2020, **39**, 1440–1447; (*b*) R. Zhang, Y. Wang, Y. Zhao, C. Redshaw, I. L. Fedushkin, B. Wu and X.-J. Yang, *Dalton Trans.*, 2021, **50**, 13634–13650.

12 X. Liu, M. Heinz, J. Wang, L. Tan, M. C. Holthhausen and Q. Ye, *Angew. Chem., Int. Ed.*, 2023, **62**, e202312608.

13 (*a*) J. Krebs, M. Haehnel, I. Krummenacher, A. Friedrich, H. Braunschweig, M. Finze, L. Ji and T. B. Marder, *Chem.–*

Eur. J., 2021, **27**, 8159–8167; (*b*) L. Xiang, J. Wang, I. Krummenacher, K. Radacki, H. Braunschweig, Z. Lin and Q. Ye, *Chem.–Eur. J.*, 2023, **29**, e202301270.

14 (*a*) J. Li, R. Pang, Z. Li, G. Lai, X.-Q. Xiao and T. Müller, *Angew. Chem., Int. Ed.*, 2019, **58**, 1397–1401; (*b*) Y. Wu, J. Zhang and Z. Xie, *Chin. Chem. Lett.*, 2019, **30**, 1530–1532; (*c*) L. Xiang, J. Wang, L. Tan and Q. Ye, *Inorg. Chem.*, 2026, **65**, 1045–1050; (*d*) S. Yao, T. Szilvási, Y. Xiong, C. Lorent, A. Ruzicka and M. Driess, *Angew. Chem., Int. Ed.*, 2020, **59**, 22043–22047; (*e*) S. Yao, A. Kostenko, Y. Xiong, A. Ruzicka and M. Driess, *J. Am. Chem. Soc.*, 2020, **142**, 12608–12612; (*f*) H. Wang, J. Zhang, H. K. Lee and Z. Xie, *J. Am. Chem. Soc.*, 2018, **140**, 3888–3891.

15 (*a*) R. G. Adler and M. F. Hawthorne, *J. Am. Chem. Soc.*, 1965, **87**, 4746–4750; (*b*) R. G. Adler and M. F. Hawthorne, *J. Am. Chem. Soc.*, 1970, **92**, 6174–6182; (*c*) C. Zhang, X. Liu, J. Wang and Q. Ye, *Angew. Chem., Int. Ed.*, 2022, **61**, e202205506; (*d*) C. Zhang, J. Wang, Z. Lin and Q. Ye, *Inorg. Chem.*, 2022, **61**, 18275–18284; (*e*) C. Zhang, J. Wang, W. Su, Z. Lin and Q. Ye, *J. Am. Chem. Soc.*, 2021, **143**, 8552–8558; (*f*) M. O. Akram, J. R. Tidwell, J. L. Dutton and C. D. Martin, *Angew. Chem., Int. Ed.*, 2023, **62**, e202307040; (*g*) L. Xiang, J. Wang, N. Knoblauch, A. Matler and Q. Ye, *Angew. Chem., Int. Ed.*, 2025, e202501955; (*h*) L. Xiang, J. Wang, A. Matler and Q. Ye, *Chem. Sci.*, 2024, **15**, 17944–17949; (*i*) M. O. Akram, J. R. Tidwell, J. L. Dutton and C. D. Martin, *Angew. Chem., Int. Ed.*, 2022, **134**, e202212073; (*j*) L. Xiang, J. Wang, A. Matler, I. Krummenacher, H. Braunschweig and Q. Ye, *Inorg. Chem.*, 2025, **64**, 25428–25435.

16 (*a*) CCDC 2504504: Experimental Crystal Structure Determination, 2026, DOI: 10.5517/ccdc.csd.cc2q24gf; (*b*) CCDC 2504505: Experimental Crystal Structure Determination, 2026, DOI: 10.5517/ccdc.csd.cc2q24hg; (*c*) CCDC 2504506: Experimental Crystal Structure Determination, 2026, DOI: 10.5517/ccdc.csd.cc2q24jh; (*d*) CCDC 2504507: Experimental Crystal Structure Determination, 2026, DOI: 10.5517/ccdc.csd.cc2q24kj; (*e*) CCDC 2504508: Experimental Crystal Structure Determination, 2026, DOI: 10.5517/ccdc.csd.cc2q24lk.